Frontiers of Information Technology & Electronic Engineering
www.jzus.zju.edu.cn; engineering.cae.cn; www.springerlink.com
ISSN 2095-9184 (print); ISSN 2095-9230 (online)
E-mail: jzus@zju.edu.cn

Review:

Rational design of semiconductor metal oxide nanomaterials for gas sensing by template-assisted synthesis: a survey*#

Yuanyang XUN§, Siqi LI†§‡, Feiyu ZHANG, Yan HONG, Ke XU, Ligang CHEN, Song LIU†, Bin LI†
MOE Key Laboratory of Forest Plant Ecology, College of Chemistry, Chemical Engineering and Resource Utilization, Northeast Forestry University, Harbin 150040, China
†E-mail: lisiqibest@sina.com; carlosliusong@nefu.edu.cn; libinzh62@163.com

Received Nov. 8, 2022; Revision accepted Feb. 22, 2023; Crosschecked Apr. 26, 2023

Abstract: Gas sensors have received extensive attention because of the gas pollution caused by rapid construction of urbanization and industrialization. Gas sensors based on semiconductor metal oxide (SMO) have the advantages of high response, excellent repeatability, stability, and cost-effectiveness, and have become extremely important components in the gas sensor field. Materials with regular structures and controllable morphology exhibit more consistent and repeatable performance. However, during the process of material synthesis, because of the uncontrollability of the microcosm, nanomaterials often show irregularities, unevenness, and other shortcomings. Thus, the synthesis of gas sensors with well-aligned one-dimensional (1D) structures, two-dimensional (2D) layered structures, and three-dimensional (3D) hierarchical structures has received extensive attention. To obtain regular structured nanomaterials with desired morphologies and dimensions, a template-assisted synthesis method with low cost and controllable process seems a very efficient strategy. In this review, we introduce the morphology and performance of SMO sensors with 1D, 2D, and 3D structures, discuss the impact of a variety of morphologies on gas sensor performance (response and stability), and shed new light on the synthesis of gas sensing materials with stable structure and excellent performance.

Key words: Gas sensors; Chemi-resistors; Template-assisted methods; Nanostructure; Dimension
https://doi.org/10.1631/FITEE.2200552 **CLC number:** X831; TP212

1 Introduction

Over recent decades, there has been a growing interest internationally in gas sensing to avoid environmental problems and human health damage. Based on the requirements for practical application, gas sensors need to have a rapid, accurate, and simple operation. Gas chromatography coupled to mass spectrometry and ion mobility spectrometry can satisfy some of these requirements.

However, these methods need a specific device, are complicated to operate, and are unsuitable for timely monitoring of harmful gases. Researchers have tried many strategies to develop various alternative types of gas sensors including optical sensors (Escobedo et al., 2022), acoustic wave sensors (Zeng G et al., 2019), thermoelectric sensors (Masoumi et al., 2019), and electrochemical sensors (Li RF et al., 2020), but their high cost and only modest improvement in performance have limited further development. Thus, there is an urgent need to find portable, efficient, and low-cost gas detection technologies to meet the increasing demand.

§ These two authors contributed equally to this work
‡ Corresponding author
* Project supported by the National Natural Science Foundation of China (No. 62001097), the Natural Science Foundation of Heilongjiang Province (No. LH2020F001), the Young Elite Scientists Sponsorship Program by China Association for Science and Technology (CAST) (No. YESS20210262), the China Postdoctoral Science Foundation-Funded Project (No. 2021M690571), the Heilongjiang Postdoctoral Fund, China (No. LBH-Z21096), and the Fundamental Research Funds for the Central Universities, China (No. 2572020BU04)
# Electronic supplementary materials: The online version of this article (https://doi.org/10.1631/FITEE.2200552) contains supplementary materials, which are available to authorized users
ORCID: Siqi LI, https://orcid.org/0000-0003-0695-9629

Resistive gas sensors are considered the most promising candidates for various applications due to their low cost and high efficiency (Liu W et al., 2018; Giampiccolo et al., 2019; Jo et al., 2021; Ogbeide et al., 2022). Using appropriate materials permits the detection of various gases, including formaldehyde, carbon monoxide, ethanol, and others (see supplementary materials, Section 1.1). Recently, semiconductor metal oxide (SMO) has become one of the most attractive gas sensing materials because of its high response, outstanding repeatability, excellent stability, and cost-effectiveness. For detailed performance parameters, see supplementary materials, Section 1.2. Table 1 lists some previous studies of resistive gas sensors based on semiconductor materials. The detection range is usually at ppm (1 ppm=1×10^{-6}) levels, and cannot be higher or lower because of the need for gases to be adsorbed and desorbed on the surface of the materials. Therefore, their morphology, such as surface area, porosity, and dimensionality, plays a crucial role in the gas sensing process. For example, zero-dimensional (0D) quantum dots, one-dimensional (1D) nanowires, two-dimensional (2D) thin films, and three-dimensional (3D) microspheres have different gas diffusion paths and adsorption modes, leading to differences in their response time and limit of detection (LOD).

Template-assisted synthesis methods are an efficient way to obtain the desired uniform morphology and structure of nanomaterials. They can be broadly classified as hard- or soft-template-assisted methods. Hard templates are mainly inorganic substances, such as silicon dioxide or metal organic frameworks (MOFs). Soft templates are primarily organic materials, such as polyvinyl pyrrolidone (PVP) or polystyrene (PS) spheres. For example, Yuan HY et al. (2019) used MOFs as a template to prepare a CO and volatile organic compound (VOC) sensor based on hierarchical ZnO sheets. This method renders excellent and repeatable gas sensing performance. Using PS microsphere 2D colloidal crystal as a template, Xu et al. (2014) designed a SnO_2 monolayer ordered porous films-based ethanol sensor. Controlling the pore size can optimize the response and stability of a gas sensor. Using polyurethane acrylate as a template, Seo et al. (2020) developed a H_2 sensor based on a self-powered Pd polyurethane acrylate (PUA) nanomaterial. The sensor can transmit the detection results immediately to a phone over Bluetooth, which is very convenient.

In this review, we summarize recent reports on state-of-the-art research that converge on template-assisted synthesis approaches for gas sensor nanomaterials. We aim to provide a better understanding of gas sensors and guide the design of high-efficiency gas sensor nanomaterials. First, the fundamental concepts of SMO gas sensors are introduced, including the detection methods and the SMO sensing mechanism (see supplementary materials, Section 1.3), which is helpful to better understand the concepts and modifications of SMO sensors. In addition, we discuss the factors affecting the materials prepared by template methods, such as the classification and selection of templates (see supplementary materials, Section 2.1), the various synthesis methods (see supplementary materials, Section 2.2), and the impact of calcination temperature (see supplementary materials, Section 2.3). Then, several template-assisted synthesis strategies are discussed in detail, highlighting nanomaterials with different dimensionality. Finally, promising developments in gas sensor technology are explained comprehensively.

Table 1 Summary of studies of semiconductor materials for gas sensing

Sensing material	Gas	Temperature	Concentration/Response	τ_{res} (s)	LOD (ppb)	Reference
rGO/$CuCoO_x$	NO_2	RT	1 ppm/64.76%	250	50	Ogbeide et al. (2022)
Pt@In_2O_3	Acetone	320 ℃	1 ppm/6.23	11	10	Liu W et al. (2018)
ZIF-7/TiO_2	Formaldehyde	RT	5 ppm/1350	9	16	Jo et al. (2021)
GO/TiO_2	NO_2	RT	1.75 ppm/3.14	35	70	Giampiccolo et al. (2019)
Pd-$BiVO_4$	3-hydroxy-2-butanone	200 ℃	10 ppm/103.7	12	200	Chen et al. (2020)
ZnO	NO_2	RT	1 ppm/29	22	0.2	Xia et al. (2020)
CeO_2-WO_3	Acetone	250 ℃	0.5 ppm/1.31	34	500	Yuan KP et al. (2020)

rGO: reduced graphene oxide; ZIF: zeolite imidazole framework; RT: room temperature; τ_{res}: response time; LOD: limit of detection. 1 ppm=1×10^{-6}; 1 ppb=1×10^{-9}

2 1D nanomaterials based on template-assisted methods

1D nanomaterials contain mainly nanorods (Nasir et al., 2014; Zhang B et al., 2021), nanofibers (Kim DH et al., 2019, 2020), or nanotubes (Xue et al., 2016; Sharma et al., 2021). The 1D geometric morphology provides abundant functional groups and a large specific surface area, which is conducive to the construction of materials with excellent chemical reactivity and mechanical properties. Also, 1D nanostructured materials exhibit excellent electrical mobility, facilitating the transport of electrons, which is favorable for gas sensing performance. Studies of gas sensors based on 1D nanomaterials materials generated by template-assisted synthesis are summarized in Table 2.

Efficient template-assisted methods for synthesizing 1D nanomaterials have three common pathways. The first is a template-assisted electrospinning method, often used to synthesize hollow nanofibers. Tie et al. (2020) fabricated praseodymium-doped $BiFeO_3$ hollow nanofibers using an electrospinning technique for formaldehyde sensing, using PVP as a soft template (Fig. 1a). The sensor had an outstanding response of 30.1 to 100 ppm formaldehyde at 190 ℃ because the tubular nanomaterials have a large surface area and pore size (Fig. 1b). Similarly, Yang JQ et al. (2021) constructed Sn-doped NiO nanofibers using the same electrospinning method as used for a triethylamine (TEA) sensor. They found that the TEA response value was about 16.6 to 100 ppm and the as-prepared nanomaterials had excellent moisture resistance (Fig. 1c). The experiments revealed that the surface state of the materials could be easily altered by the doped Sn due to the 1D structure. Furthermore, with apoferritin as the template, Shin et al. (2021) reported Na-doping and Pt nanoparticle (NP) decorating of WO_3 nanofibers using an electrospinning process. The H_2S sensing performance exceeded that of previous reports, reaching 780 at 1 ppm. The H_2S concentration threshold for halitosis in the mouth was estimated with excellent stability to be about 150 ppb (1 ppb=1×10^{-9}) by this sensor. The device can be used for medical detection with an accuracy of 86.3% (Fig. 1d). The study indicated that the 1D structure played an important role in the outstanding response and selectivity for H_2S. Sanger et al. (2018) used PVP nanofibers as a hard template to synthesize free-standing hollow aluminum-doped zinc oxide nanofibers. Compared with filled fibers (~6/3 min), hollow fibers showed slower response/recovery time (~11/10 min) and a higher response. The response/recovery time of gas NO_2 sensing could be explained by the diffusion kinetics and penetration depth. They used finite-difference time-domain (FDTD) simulation to calculate the distribution of the active area field at different temperatures. Gas molecules are adsorbed only on the surface of nanomaterials. Thus, the gas NO_2 cannot diffuse through the aluminum-doped zinc oxide (AZO) layer of filled fibers, resulting in a faster adsorption–desorption and response–recovery time. In contrast, the gas NO_2 can pass through the tubes of hollow fibers and produce more collisions in the tube. Compared with the outer surface, the collision frequency is almost eight times higher inside the core at 25 ℃ (Figs. 1e and 1f). Therefore, hollow fibers have better gas sensing performance. This was the first time the gas response mechanism of hollow nanofibers had been proposed. The material showed an excellent sensing response to low concentration NO_2 gas at room temperature,

Table 2 Summary of studies of one-dimensional (1D) nanomaterials for gas sensing by template-assisted methods

Template	Sensing material	Gas	Temperature (℃)	Concentration/Response	τ_{res} (s)	Reference
PVP	$BiFeO_3$	Formaldehyde	190	100 ppm/30.1	19	Tie et al. (2020)
Apoferritin	Pt-WO_3	H_2S	300	1 ppm/780	10	Shin et al. (2021)
MgO microrods	Co_3O_4	Triethylamine	180	200 ppm/220%	13	Hu et al. (2022)
$ZnFe_2(C_2O_4)_3$	$ZnFe_2O_4$	Acetone	260	100 ppm/52.8	1	Li L et al. (2017)
Shaddock peel	Cd-SnO_2	Formaldehyde	160	100 ppm/51.11	28	Zhao RJ et al. (2020)
Absorbent cotton	α-Fe_2O_3/$Fe_2(MoO_4)_3$	H_2S	133	10 ppm/12.69	3	Wu et al. (2021)
Absorbent cotton	ZnO	H_2S	217	10 ppm/85.04	8	Na et al. (2019b)
Absorbent cotton	CuO/ZnO	H_2S	170	500 ppb/2.19	27	Na et al. (2019a)

τ_{res}: response time. 1 ppm=1×10^{-6}; 1 ppb=1×10^{-9}

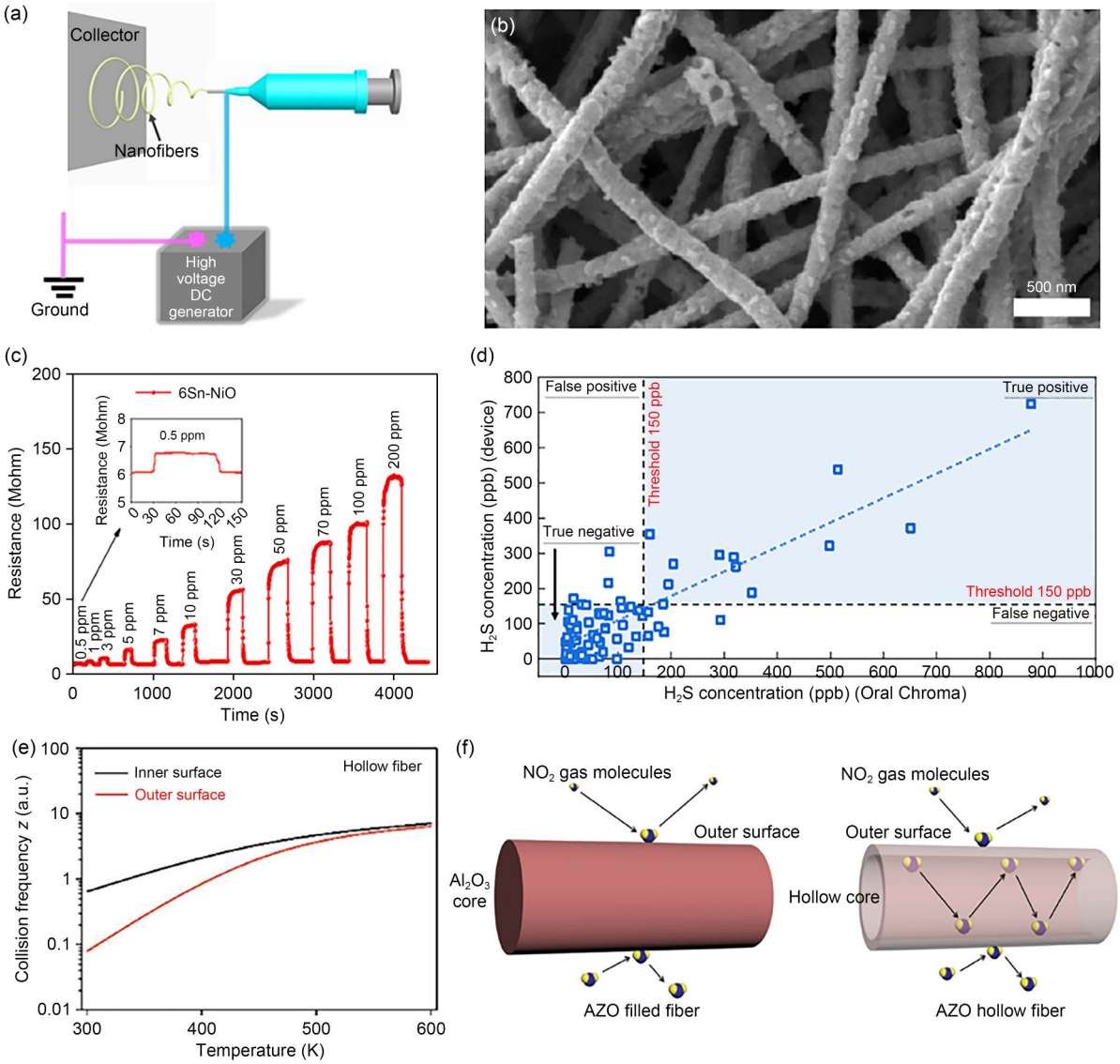

Fig. 1 Schematic of the basic setup for electrospinning (a), a scanning electron microscope (SEM) image of Pr-doped $BiFeO_3$ (b), dynamic response curves of the sensors based on Sn-NiO to triethylamine (TEA) at 180 °C (c), correlation between H_2S concentration measured and calculated by the Oral Chroma device (d), collision frequency versus temperature for the outer and inner surfaces of the hollow fiber (e), and interaction between the filled fibers and the hollow fibers (f)

(a) and (b) are reprinted from Tie et al. (2020), Copyright 2020, with permission from Elsevier; (c) is reprinted from Yang JQ et al. (2021), Copyright 2021, with permission from Elsevier; (d) is reprinted from Shin et al. (2021), Copyright 2021, with permission from American Chemical Society; (e) and (f) are reprinted from Sanger et al. (2018), Copyright 2018, with permission from the authors, licensed under CC BY. DC: direct current; AZO: aluminum-doped zinc oxide. 1 ppm=1×10^{-6}; 1 ppb=1×10^{-9}

which depended on its high surface-to-volume ratio. The study developed a new strategy using a template-assisted synthesis method to prepare 1D nanostructures for gas sensor applications.

The second pathway is the self-template method. Material is grown with the help of the template, and then the template is removed to obtain the 1D nanomaterial. With this approach, Baek et al. (2019) reported suspended nanowires (PdO, NiO, SnO_2, and WO_3) using suspended carbon nanotubes (CNTs) as a self-template (Fig. 2a). A scanning electron microscope (SEM) image of a nanowire is shown in Fig. 2b. The nanowires show a 21.9% response to 2% air-diluted H_2 gas. The authors stated that the fabrication method could realize scalable processes without any contamination. In addition, Hu et al. (2022) designed hierarchical

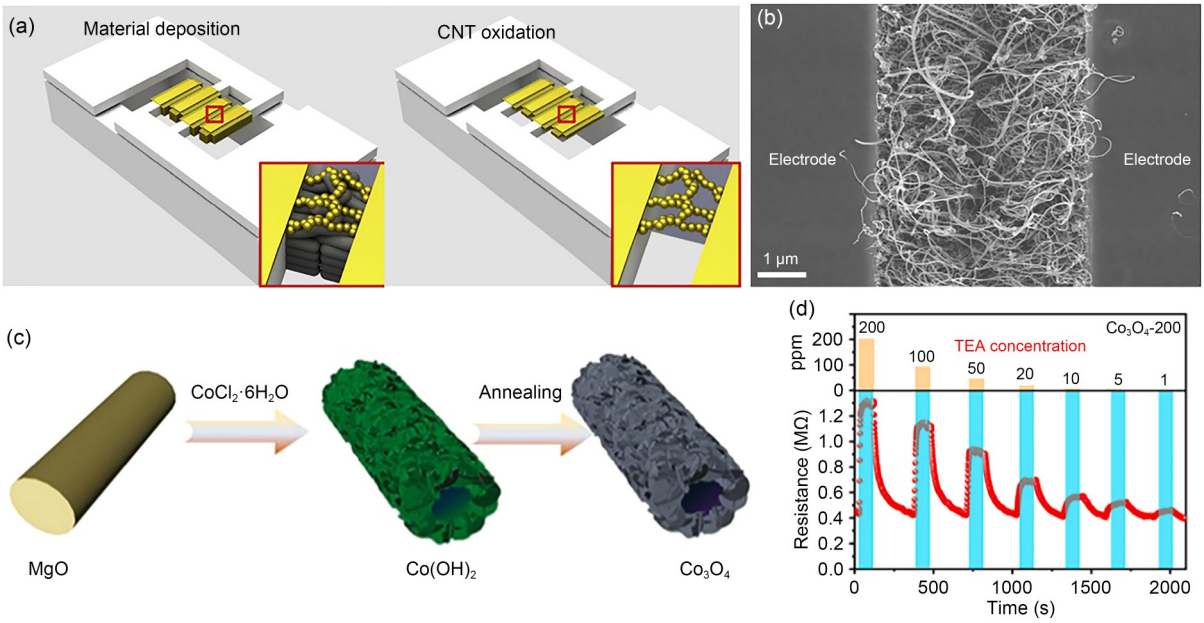

Fig. 2 Schematic showing the formation of suspended nanowires using a carbon nanotube (CNT) template (a), a scanning electron microscope (SEM) image of a nanowire remaining after calcination at 600 ℃ (b), schematic of the fabrication process for nanosheet-assembled Co_3O_4 microtubes (c), and dynamical response–recovery curve and response value of Co_3O_4 to different concentrations of triethylamine (TEA) at 180 ℃ (d)

(a) and (b) are reprinted from Baek et al. (2019), Copyright 2018, with permission from Elsevier; (c) and (d) are reprinted from Hu et al. (2022), Copyright 2021, with permission from Elsevier. 1 ppm=1×10^{-6}

Co_3O_4 microtubes using MgO microrods as a self-template. Fig. 2c depicts the template synthesis process. TEA can be detected by the Co_3O_4 microtubes, which exhibit a low detection limit (1 ppm) and fast recovery time (13 s) to TEA at 180 ℃ (Fig. 2d). These sensors' excellent performance is ascribed to their large surface area, rich oxygen vacancies, and suitable pore size. Furthermore, Li L et al. (2017) synthesized a porous $ZnFe_2O_4$-based nanorod acetone sensor with a networked nanostructure using the $ZnFe_2(C_2O_4)_3$ as a self-template. The response time, recovery time, and response to 100-ppm acetone were 1 s, 11 s, and 52.8, respectively. The porous $ZnFe_2O_4$ nanorods provide a large specific surface area (82.01 m^2/g) and more active sites on the surface. Overall, the self-template method is an excellent method for preparing 1D nanomaterials.

In addition, some natural biomaterials have an exclusive hierarchical structure and offer a wide range of sources and minimal processing costs. Researchers can use common biomass resources as templates to create 1D nanomaterials. Shaddock (pomelo) peels can be used as bio-templates to create a unique 1D structure. Zhao RJ et al. (2020) used shaddock peels as a plant template to make a formaldehyde sensor based on Cd-doped SnO_2 nanofibers. The sensor had a strong selectivity and a high response (51.11 toward 100 ppm formaldehyde). Using shaddock peels as a template to synthesize 1D nanomaterials is a promising method. A popular research area is using absorbent cotton as a template to create 1D nanomaterials. Gas transmission is assisted by the hierarchically porous tubular structure inherited from absorbent cotton. In a recent study, Wu et al. (2021) used absorbent cotton as a template to synthesize an α-Fe_2O_3/$Fe_2(MoO_4)_3$ microtubule based H_2S sensor. The sensor has outstanding response and selectivity to trace H_2S due to the synergy of inherent features of porous microtubules. In addition, Na et al. used absorbent cotton as a template to make hierarchically porous ZnO hollow nanotubes (Na et al., 2019b) and porous CuO/ZnO heterostructural tubules (Na et al., 2019a) by impregnating them with a precursor salt solution by calcining at high temperatures. Fig. 3a depicts the bio-template synthesis process. The clean fiber microstructure of absorbent cotton and the high number of cross-linked NPs with small holes aggregated into the hexagonal hollow tubular structure are well preserved in the morphologies of ZnO hollow

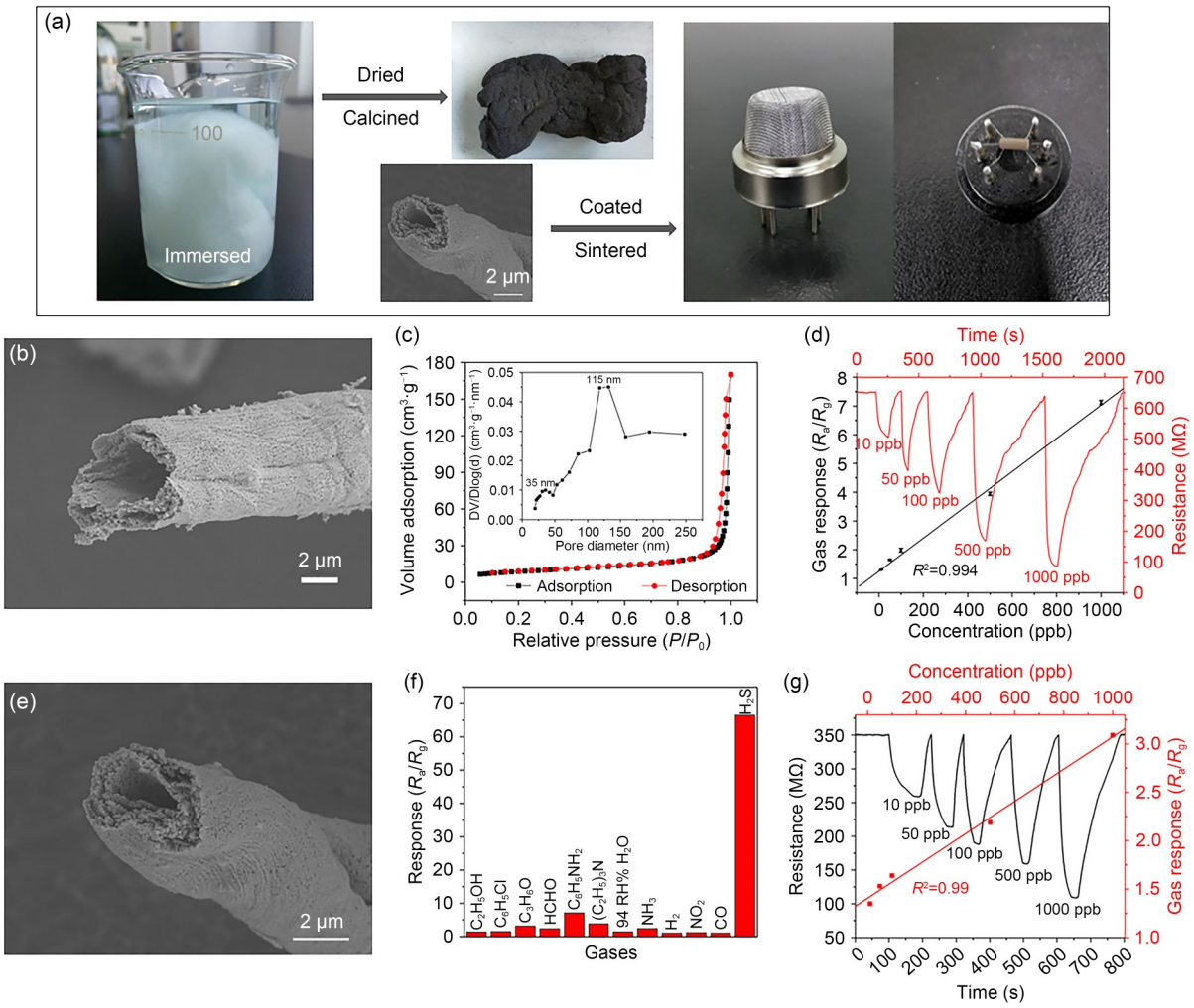

Fig. 3 Schematic of the process for synthesizing porous hollow nanotubes (a), a scanning electron microscope (SEM) image of a ZnO nanotube (b), nitrogen adsorption–desorption curve and pore size distribution of a ZnO gas sensor (c), response–recovery characteristics and responses of a ZnO gas sensor to H_2S at 217 ℃ (d), an SEM image of a CuO/ZnO heterostructural tubule (e), response of a CuO/ZnO gas sensor to different gases at 217 ℃ (f), and response–recovery characteristics and the responses of a CuO/ZnO gas sensor to H_2S at 170 ℃ (g)

(a) and (e)–(g) are reprinted from Na et al. (2019a), Copyright 2019, with permission from Elsevier; (b)–(d) are reprinted from Na et al. (2019b), Copyright 2019, with permission from American Chemical Society. 1 ppb=1×10^{-9}

nanotubes (Fig. 3b) and CuO/ZnO tubules (Fig. 3e). Fig. 3c shows the nitrogen adsorption–desorption isotherms and pore size distribution of ZnO nanotubes. The pore size of the nanotubes is centered at 115 nm, with a specific surface area of 31 m^2/g. The ZnO nanotube sensor has a high response to H_2S with a good linear relationship for a concentration range of 10–1000 ppb (Fig. 3d). The sensor also has a rapid response time of 29 s when exposed to 50 ppb H_2S gas. Figs. 3f and 3g show the sensing performance of a CuO/ZnO-based sensor to H_2S, demonstrating high selectivity, a low detection limit of 10 ppb H_2S (1.34), and a wide linear range. This new strategy based on the use of an absorbent cotton template allows for the creation of highly active NPs.

As a common laboratory item, cellulose filter paper can be used as a template to synthesize 1D nanomaterials. Ivanova et al. (2020) demonstrated a method for preparing porous SnO_2 films using a simple wet-chemical technique (Fig. 4a) and a cellulose filter paper as a template. The sensor based on a porous SnO_2 film (Fig. 4b) has outstanding sensing response and a fast response to CO (3 s) at a low operating temperature (Fig. 4c). Candle soot has a fractal structure with a large

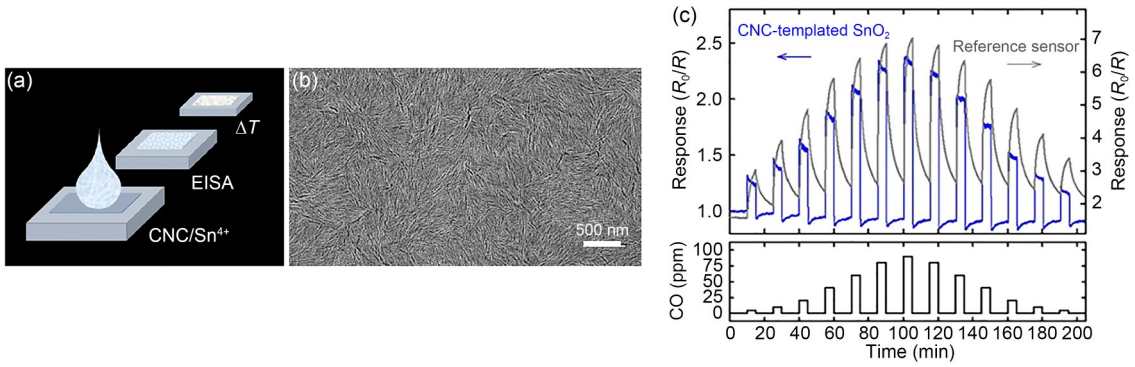

Fig. 4 Schematic of the process for fabricating SnO_2 thin films (a), a scanning electron microscope (SEM) top-view image of SnO_2 thin films (b), and response of the cellulose nanocrystal (CNC)-templated SnO_2 CO sensor to CO gas at 350 °C and 50% relative humidity (RH) (c)

Reprinted from Ivanova et al. (2020), Copyright 2020, with permission from American Chemical Society. EISA: evaporation-induced self-assembly. 1 ppb=1×10^{-9}

surface area and excellent water/oil repellency, making it a good template for making 1D nanomaterials.

The 1D nanomaterials synthesized using a template have a large specific surface area and provide a large number of active reaction sites, which accelerates the resistance change. This type of material has a lot of potential in terms of applications.

3 2D nanomaterials based on template-assisted methods

Carrier migration and heat diffusion are confined to the planes in 2D nanomaterials. 2D nanomaterials are appropriate for the production of gas sensors due to their large specific surface area, excellent carrier mobility, and large number of adsorption sites. The potential of 2D nanomaterials should not be overlooked. However, fabricating 2D nanomaterials using a simple, pollution-free, and low-cost process remains a significant challenge. There are many ways to create 2D materials (Sun et al., 2014; Tan and Zhang, 2015). The synthesis of gas sensors based on 2D nanomaterials using a template-assisted method is relatively rare nowadays, but their performance is excellent (Ma et al., 2020; Wen et al., 2023). Hence, innovative methods for preparing 2D nanomaterials prepared by templates are worth investigating. Studies of gas sensors based on 2D nanomaterials generated by template-assisted synthesis are summarized in Table 3.

For example, Sabri et al. (2018) developed a porous TiO_2 acetone sensor, made by depositing TiO_2 shells on a soot template. The fabrication process is shown in Fig. 5a. TiO_2 layers maintained the distinctive integrated structure that soot templates provide (Fig. 5b). Under ultraviolet (UV) illumination, the TiO_2-based sensor has a low detection limit of 10 ppb, a high reaction rate, and strong selectivity performance (Fig. 5c), demonstrating the potential of applications for non-invasive lung cancer exhalation diagnosis. Biomass material can be used as a suitable template for fabricating 2D nanomaterials. A common biological template that can be used to create 2D materials is the leaf. Using tree leaves as templates, Liu WX et al. (2023) synthesized Fe_2O_3 nanosheets with a wide pore distribution. Their microstructural characteristics help increase gas response. Liu XJ et al. (2022) developed a p-xylene sensor based on 2D hierarchical CeO_2 nanosheets using tree leaves as a template. The template material features a unique cross-linked NP structure with high crystallinity, large specific surface area, and consistent pore size distribution.

2D materials can also be prepared from common high molecular weight polymers, such as PS spheres. When PS spheres are horizontally stacked on a PS plane, they can be used as templates to prepare high-quality and uniform 2D materials. Using PS spheres as templates, Lu et al. (2017) showed a promising method to improve the sensing performance. The organic field effect transistor-based sensors showed better NH_3 detection performance than materials without templates. Luong et al. (2021) used PS spheres as a template to make a PdCo NP/polymethyl methacrylate (PMMA) nanomaterial-based H_2 room temperature

Table 3 Summary of studies of two-dimensional (2D) nanomaterials for gas sensing by template-assisted methods

Template	Sensing material	Gas	Temperature (°C)	Concentration/Response	τ_{res} (s)	Reference
Sponge	In_2O_3	Cl_2	200	3 ppm/2353.4	53	Ma et al. (2020)
rGO	$ZnFe_2O_4$	Acetone	220	50 ppm/64.9	23	Wen et al. (2023)
Filter paper	SnO_2	CO	350	90 ppm/2.4	3	Ivanova et al. (2020)
Soot	TiO_2	Acetone	325	12.5 ppm/98.7%	12	Sabri et al. (2018)
Tree leaves	CeO_2	P-xylene	170	1 ppm/16.5	74	Liu XJ et al. (2022)
Tree leaves	Fe_2O_3	Butanone	170	100 ppm/25.8	5	Liu WX et al. (2023)
PS spheres	W-NiO	NO_2	300	5 ppm/200	2	Yi et al. (2019)
PS spheres	$BiVO_4$	H_2S	75	5 ppm/4.9	5	Li C et al. (2019)
Salt crystals	CeO_2/SnO_2	3-hydroxy-2-butanone	160	50 ppm/623	29	Yang XY et al. (2022)
Salt crystals	Si-WO_{3-x}	Acetone	175	50 ppm/119	21	Xie et al. (2021)

rGO: reduced graphene oxide; PS: polystyrene; τ_{res}: response time. 1 ppm=1×10^{-6}

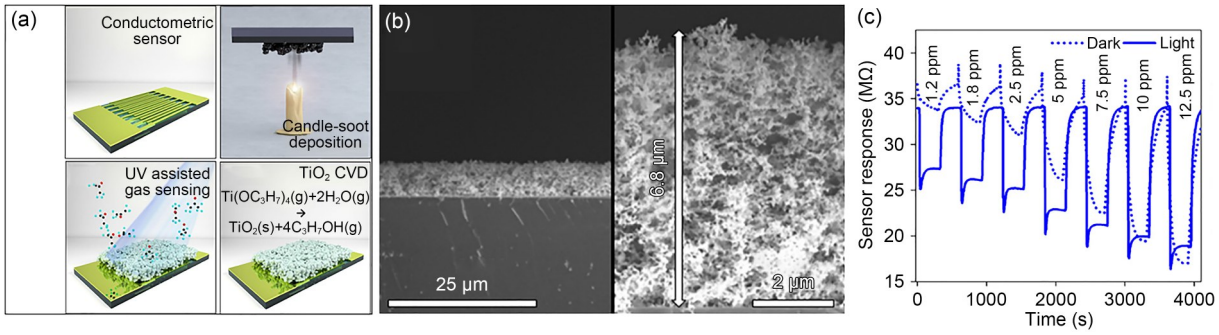

Fig. 5 Schematic of the fabrication process of a soot template TiO_2 gas sensor (a), different magnification scanning electron microscope (SEM) images showing the uniformity and thickness of the surface of a SnO_2 sensor device (b), and dynamic response curve of the SnO_2 gas sensor to different acetone concentrations (c)

Reprinted from Sabri et al. (2018), Copyright 2018, with permission from Elsevier. UV: ultraviolet; CVD: chemical vapor deposition. 1 ppm=1×10^{-6}

sensor (Fig. 6a). Fig. 6b shows a cross-sectional SEM image of the NPs. At room temperature, the sensor has a very fast response time (0.85 s) and excellent protection against various interfering gases (CH_4, CO_2, and CO) (Figs. 6c and 6d). Yi et al. (2019) developed a NO_2 sensor based on the heterojunction of W-NiO nanoigloos that evolved morphologically using PS spheres as a template. This sensor shows excellent response and selectivity to NO_2 gas. In addition, thick film structures can be synthesized. Li C et al. (2019) prepared a H_2S sensor based on ordered porous $BiVO_4$ multilayer thick films using PS spheres as templates (Fig. 6e). $BiVO_4$ films have honeycomb-like microstructures that are highly ordered and close-packed. A sample with a diameter of 200 nm provides the largest number of active sites and a large surface area, enhancing the use of the entire structure and ensuring a fast response and recovery rate (Fig. 6f), a low detection limit (62.5 ppb), and excellent sensor selectivity (Fig. 6g).

Salt crystals can also be used as templates to synthesize 2D materials. Yang XY et al. (2022) reported a method for creating crystalline porous CeO_2/SnO_2 nanosheets using salt crystals (such as KCl and KBr) as a template. The sensors based on this material have outstanding 3-hydroxy-2-butanone gas sensing performance. Using scalable carbonate crystals as a template, Xie et al. (2021) prepared the unique Si-WO_{3-x} with a large available surface area and abundant oxygen vacancies. The nanosheets are simple to assemble into a nanoflower structure, and the ultra-thin structure helps enhance their ability to detect acetone.

4 3D nanomaterials based on template-assisted methods

3D nanomaterials generally have a large specific surface area, a stable structure, and good gas diffusion, making them ideal for use as gas sensitive materials.

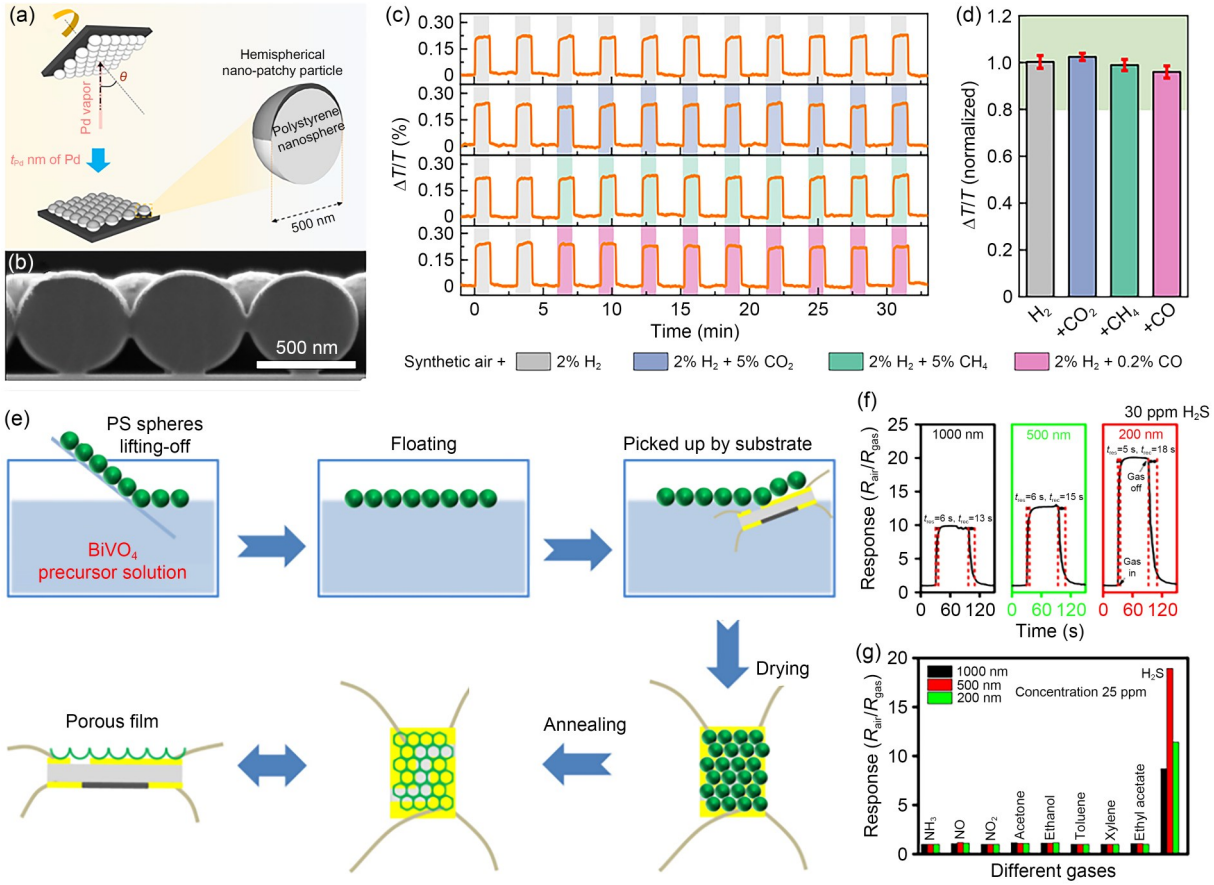

Fig. 6 Schematic of the process for fabricating PdCo NP/PMMA nanomaterials (a), a cross-sectional scanning electron microscope (SEM) image of NPs (b), response of PdCo NPs to 2% H_2, 2% H_2+5% CH_4, 2% H_2+5% CO_2, and 2% H_2+0.2% CO (c), the standard deviation from 2% H_2 (d), schematic of the procedure for preparation of an ordered porous $BiVO_4$ gas sensor (e), characteristic curves toward 30 ppm H_2S (f), and response of gas sensors based on different thickness to 25 ppm of different gases (g)

(a)–(d) are reprinted from Luong et al. (2021), Copyright 2021, with permission from the authors, licensed under CC BY 4.0; (e)–(g) are reprinted from Li C et al. (2019), Copyright 2019, with permission from Elsevier. NP: nanoparticle; PMMA: polymethyl methacrylate; PS: polystyrene. 1 ppm=1×10^{-6}

Template-assisted synthesis methods have the potential to produce 3D nanomaterials. Carbonaceous templates (Shin and Lee, 2016), SiO_2 spheres (Huang et al., 2013; Lin et al., 2017), PS spheres (Zhu et al., 2018; Fei et al., 2020), and MOFs (Liang et al., 2019; Zhao C et al., 2021) are all suitable templates for 3D nanomaterial (Fig. 7). Studies of gas sensors based on 3D nanomaterials generated by template-assisted synthesis are summarized in Table 4.

4.1 Carbonaceous templates

A carbonaceous template has a high degree of rigidity, making it an ideal self-template that is frequently used to construct spherical structures. The morphology of the replacement is stable after calcination, and the particle size can be controlled. The carbon comes from a variety of low-cost sources, such as glucose and sucrose (Yao et al., 2017; Cheng et al., 2021). For instance, Wang Q et al. (2021) used a hydrothermal technique to develop an acetone gas sensor based on egg yolk-shell Sb_2O_3/WO_3 using carbon spheres as a template. This sensor has an ultrafast sensing response and recovery time of 4 s/5 s to 100 ppm acetone. Xiong et al. (2018) synthesized multi-shelled $ZnCo_2O_4$ yolk-shell spheres and used glucose as a carbon source. The sensor has a 38.2 reaction to 500 ppm acetone and a response time of 19 s. Furthermore, Zheng YY et al. (2021) developed a xylene sensor based on multi-shelled $NiCo_2O_4$ hollow spheres (HSPs) using a simple post-annealing procedure with carbon spheres

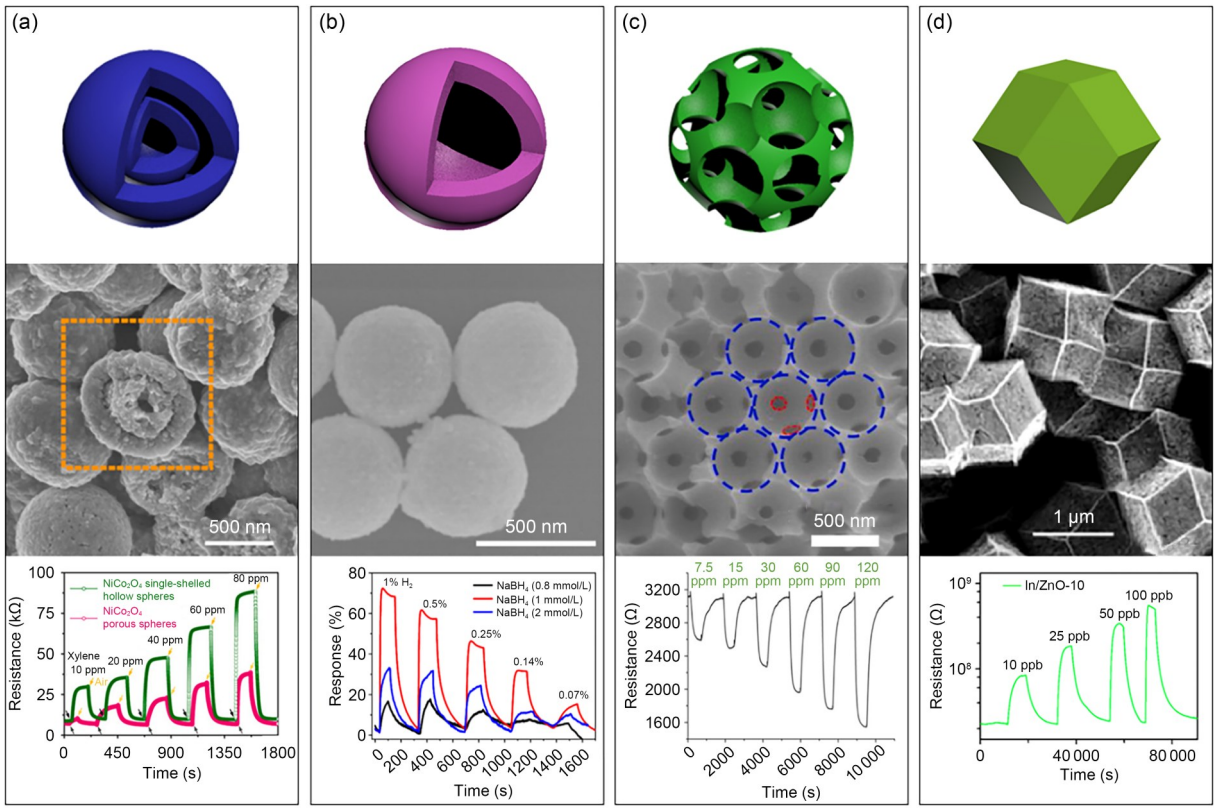

Fig. 7 Structure, scanning electron microscope (SEM) image, and gas sensing performance of various semiconducting metal oxide 3D nanostructures prepared by glucose (a), SiO_2 spheres (b), polystyrene (PS) spheres (c), and zeolite imidazole framework (ZIF)-8 (d)

(a) is reprinted from Zheng YY et al. (2021), Copyright 2021, with permission from Elsevier; (b) is reprinted from Gao et al. (2020), Copyright 2020, with permission from American Chemical Society; (c) is reprinted from Hung et al. (2020), Copyright 2020, with permission from Elsevier; (d) is reprinted from Li Z et al. (2020), Copyright 2020, with permission from American Chemical Society. 1 ppm=1×10^{-6}; 1 ppb=1×10^{-9}

Table 4 Summary of studies of three-dimensional (3D) nanomaterials for gas sensing by template-assisted methods

Template	Sensing material	Gas	Temperature (°C)	Concentration/Response	τ_{res} (s)	Reference
Carbon spheres	$NiCo_2O_4$	Xylene	240	100 ppm/23.3	15.4	Zheng YY et al. (2021)
Carbon spheres	Sb_2O_3/WO_3	Acetone	200	100 ppm/49.8	4	Wang Q et al. (2021)
SiO_2 spheres	Pt-SnO_2	H_2S	250	1 ppm/10.8	192.4	Bulemo et al. (2018)
PS spheres	$BiVO_4$	H_2S	75	5 ppm/4.9	5	Li C et al. (2019)
PS spheres	Sb-$ZnFe_2O_4$	N-butanol	250	100 ppm/35.5	4	Lv et al. (2020)
ZIF-67	Au-Co_3O_4	Acetone	190	100 ppm/14.5	319	Li Z et al. (2021)
ZIF-8	In/ZnO	NO_2	300	1 ppm/185.8	1055	Li Z et al. (2020)
ZIF-8	PdO-ZnO-In_2O_3	Triethylamine	250	50 ppm/386	1	Guo et al. (2021)
Sorghum straw	NiO-ZnO	N-butanol	330	100 ppm/54.4	4	Zeng QR et al. (2020)
Maize straw	ZnO:Ni	Acetone	340	100 ppm/68	6	Zhang XM et al. (2017)

PS: polystyrene; ZIF: zeolite imidazole framework; τ_{res}: response time. 1 ppm=1×10^{-6}

as templates (Fig. 8a). The structure of $NiCo_2O_4$ is regular and uniform, with the heating rate controlling the number of shells. The $NiCo_2O_4$ double-shelled hollow spheres (DHSs) shown in Fig. 8b are formed at a heating speed of 10 °C/min. The fabricated material has a large surface area (93.5 m^2/g) and provides more reactive sites, which can expedite the diffusion of xylene gas molecules (Fig. 8c). The results from gas-sensing showed that the $NiCo_2O_4$ DHS-based sensor has an excellent capability to sense xylene,

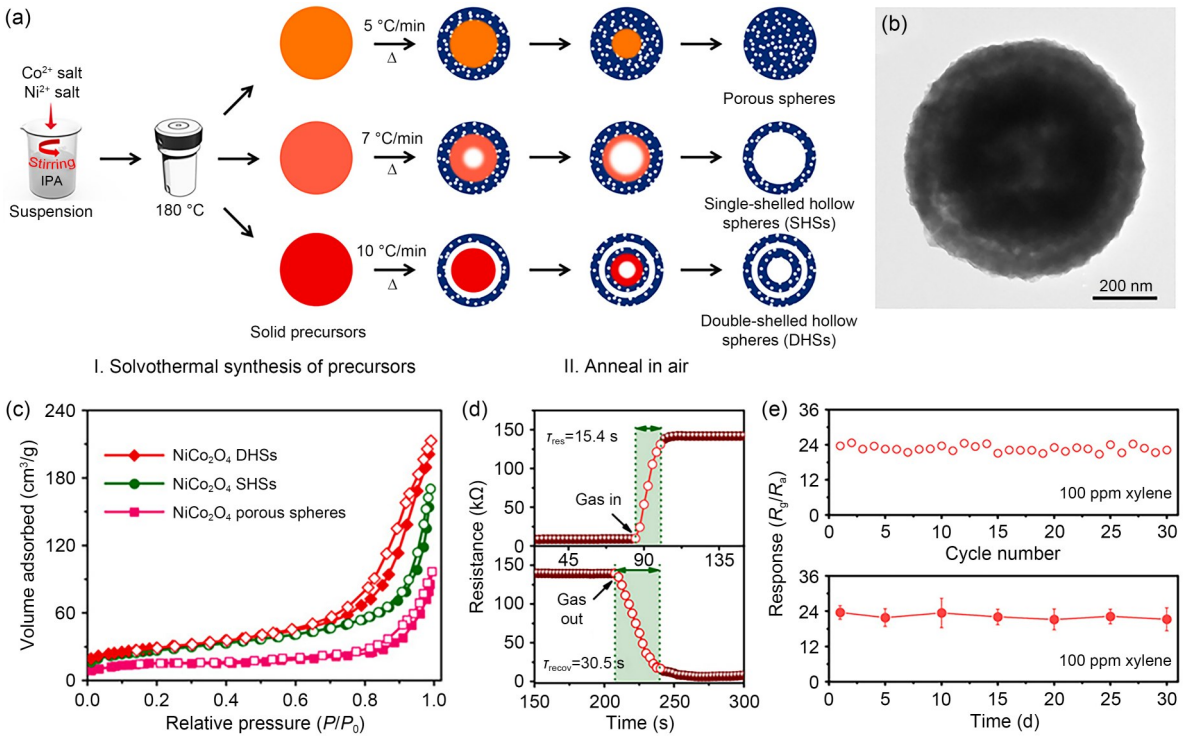

Fig. 8 Schematic of the formation of $NiCo_2O_4$ DHSs (a), a field emission scanning electron microscope (FESEM) image of $NiCo_2O_4$ DHSs (b), nitrogen adsorption and desorption isotherms of $NiCo_2O_4$ nanomaterials (c), response and recovery time of $NiCo_2O_4$ DHSs (d), and repeatability and long-term stability of $NiCo_2O_4$ DHSs to 100 ppm xylene (e)

Reprinted from Zheng YY et al. (2021), Copyright 2021, with permission from Elsevier. 1 ppm=1×10^{-6}

including a fast response and recovery characteristic, as well as a high cycle repeatability and long-term stability (Figs. 8d and 8e).

4.2 SiO_2 spheres template

Like carbon spheres, SiO_2 is commonly used as a template to manufacture 3D porous hollow materials (Huang et al., 2013; Lin et al., 2017). The material is wrapped around the surface of the SiO_2 spheres for growing, giving the structure uniformity and stability inherited from the template. As a result, researchers focused their efforts on synthesizing 3D nanomaterials using SiO_2 as a template for the construction of gas sensors. For example, Bulemo et al. (2018) used SiO_2 as a template to prepare a Pt-SnO_2 core-shell structure based hollow sphere sensor by an electrospray method. The SiO_2 was then etched away with NaOH solution to obtain SnO_2 hollow spheres with small crystallites (15.5 nm) and a large specific surface area (124.8 m^2/g). The synthesis process is shown in Fig. 9a. The Pt-SnO_2 core-shell is now considered an appropriate sensitive material for use in H_2S detection of halitosis. Using SiO_2 spheres as a template, Gao et al. (2020) designed a H_2 sensor with a Pd-modified PdO hollow shell (HS). Changing the concentration of $NaBH_4$ allows adjustment of the particle size and density of Pd NPs on the surface of the PdO DHSs, preventing Pd NP agglomeration (Fig. 9b). A transmission electron microscope (TEM) image of PdO HSs is shown in Fig. 9c. Because of its homogeneous structure, it offers strong detection performance at low H_2 concentrations of 1 ppm (Fig. 9d) and remains stable for several months. Furthermore, the sensing performance of Pd/PdO HSs can be reactivated through oxidation and $NaBH_4$ reduction.

4.3 High molecular weight polymer templates

High molecular weight polymers, such as PS spheres (Kim S et al., 2021; Wang H et al., 2022) and PMMA (Zhang LH et al., 2017; Tammanoon et al., 2020), have the advantages of uniform size, easy removal, and self-assembly, making them suitable for the preparation of regular 3D nanomaterials, such as hollow spherical structural nanomaterials and 3D inverse opal (3DIO) structural materials. For example,

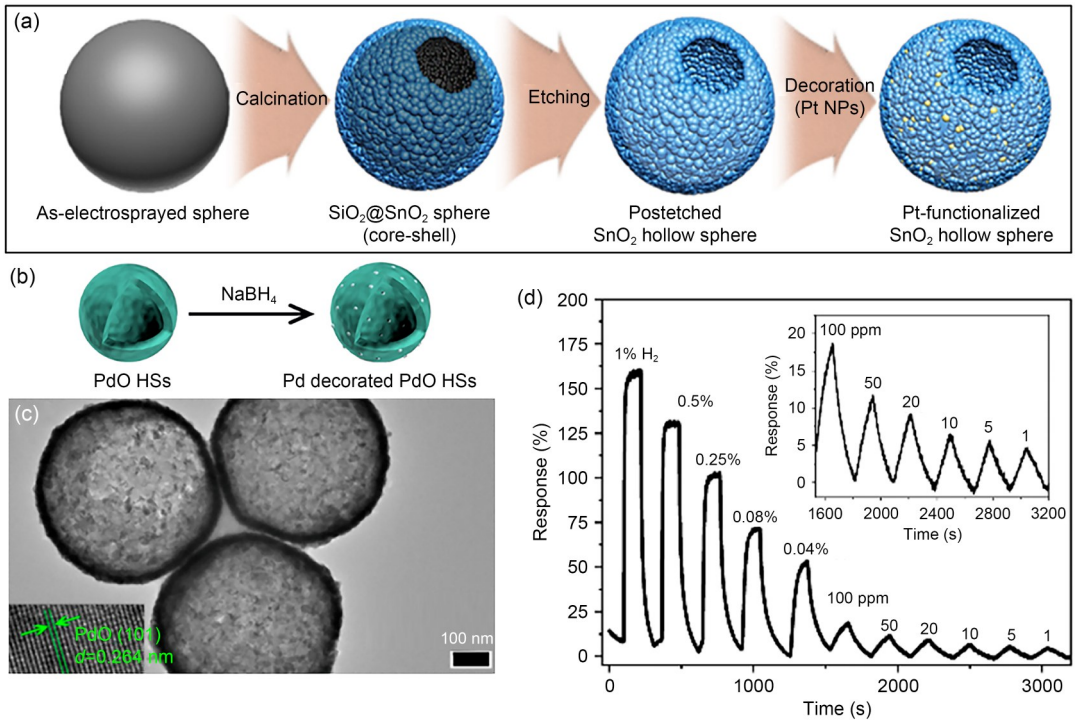

Fig. 9 Schematic of the process for synthesizing Pt-SnO_2 hollow spheres (a), PdO double-shelled hollow spheres (DHSs) treated with $NaBH_4$ (b), a transmission electron microscope (TEM) image of PdO hollow shells (HSs) (c), and real-time response of PdO HS-based H_2 sensor at 25 ℃ and relative humidity (RH) of ~50% (d)

(a) is reprinted from Bulemo et al. (2018), Copyright 2018, with permission from American Chemical Society; (b)–(d) are reprinted from Gao et al. (2020), Copyright 2020, with permission from American Chemical Society. NP: nanoparticle. 1 ppm=1×10^{-6}

Park et al. (2020) developed a SnO_2 hollow sphere based sensor with dual selectivity using PS spheres as templates. Sensors based on Au-SnO_2 nanomaterial were prepared by layering Au clusters on the inner or outer shell surface of a SnO_2 HS, allowing for the selective detection of xylene or ethanol by adjusting the configurational distributions of Au catalysts. The Au@SnO_2 sensor has a good response of 624.8 to 5 ppm p-xylene at 275 ℃, while the SnO_2@Au sensor has a good response of 504.5 to 5 ppm ethanol at 275 ℃ (Fig. 10). The study demonstrated the potential of nanomaterials with novel gas selectivity for indoor air quality monitoring applications.

Because of their ease of self-assembly, high molecular weight polymers are frequently used to prepare 3DIO structures (Zheng XZ et al., 2020; Wang L et al., 2022). The well-aligned interconnected porous structure of 3DIO provides more active sites and gas diffusion channels. By sacrificing self-assembly sulfonated PS spheres, Lv et al. (2020) created an n-butanol sensor based on 3DIO $ZnFe_2O_4$ spheres. The large number of active sites provided by the macroporous structure accelerates gas molecule diffusion and reaction, resulting in a response time of 4 s to 100 ppm n-butanol at 250 ℃. Wang TS et al. (2019) used sulfonated PS spheres as a template to fabricate 3DIO Ga-In_2O_3 microsphere-based formaldehyde sensors (Fig. 11a). Fig. 11b shows an SEM image of 3DIO Ga-In_2O_3 microspheres. The sensor achieves a high response (48.8) to 100 ppm formaldehyde and excellent gas sensing performance in the low concentration range due to its unique morphology (Figs. 11c and 11d). Hung et al. (2020) prepared a sandwiched 3DIO hierarchical structure ZnO-based H_2 sensor using electrophoresis and electrochemical deposition techniques. The sensor responds to 1.21 to 7.5 ppm H_2. Using PMMA as a template, Yang S et al. (2020) developed a H_2S sensor based on the long-range ordered 3DIO MOF ZnO@Au/WO_3. The skeleton of the WO_3/ZnO@Au is visible, and the structure is macroporous. The MOF ZnO@Au/WO_3 based sensor demonstrated an excellent response to H_2S (175 to 10 ppm target gas) at 170 ℃ due to the compositional designs and rational structure.

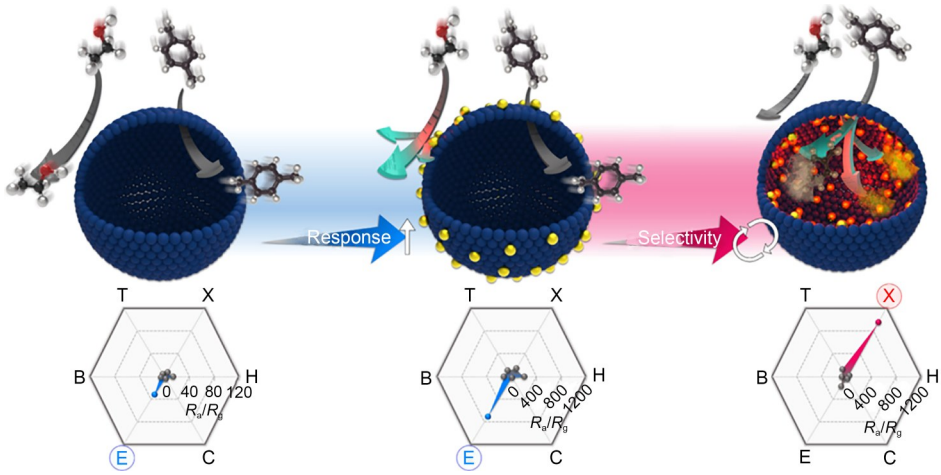

Fig. 10 Schematic of pure SnO_2, SnO_2@Au, and Au@SnO_2 hollow spheres and their gas sensing performance (ethanol, p-xylene, toluene, benzene, and formaldehyde)

Reprinted from Park et al. (2020), Copyright 2020, with permission from American Chemical Society

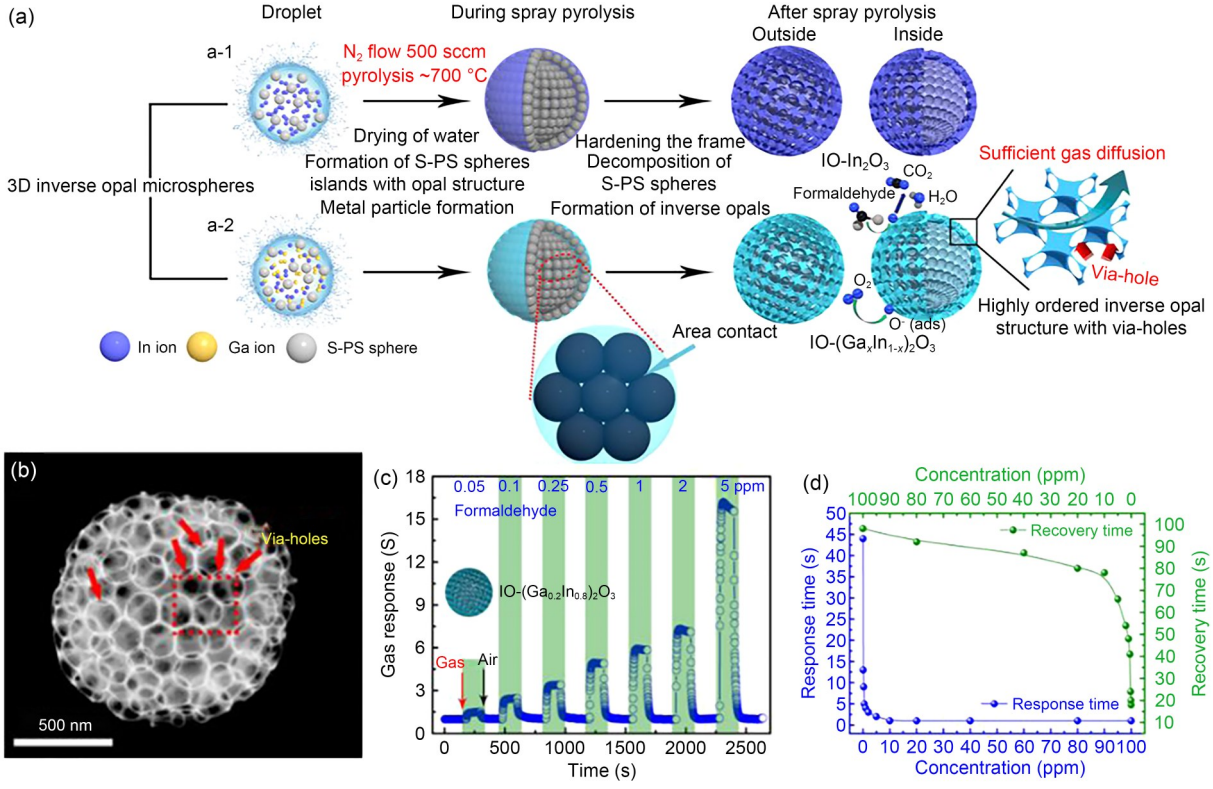

Fig. 11 Schematic illustrating the fabrication of IO-In_2O_3 and Ga-doped IO-In_2O_3 microspheres (a), a scanning electron microscope (SEM) image of IO-$(Ga_{0.2}In_{0.8})_2O_3$ (b), dynamic sensing transients to 0.05–5 ppm formaldehyde (c), and response time and recovery time to 0.05–100 ppm formaldehyde (d)

Reprinted from Wang TS et al. (2019), Copyright 2019, with permission from American Chemical Society. 1 ppm=1×10^{-6}

4.4 Metal organic framework (MOF) templates

An MOF is a type of hybrid organic–inorganic material. Intramolecular pores generate a 3D expansion of space through self-assembly of organic ligands and metal ions or clusters through coordination bonds. MOFs have a large specific surface area and a lot of active sites because of their porosity. In addition, the material's relatively high crystallinity and ordered

periodic arrangement help improve the receptor function. Therefore, the use of MOFs as templates to build 3D porous gas sensing materials has become popular in the field of gas sensors (Jang et al., 2017; Li Q et al., 2018).

Because of its well-rhombohedral structure, a zeolite imidazole framework-67 (ZIF-67) is a viable self-template for creating hollow nanostructures. For instance, Li Z et al. (2021) constructed an acetone sensor based on Au-loaded Co_3O_4 porous hollow nanocages using ZIF-67 as a template. The sensor's high response of 14.5 to 100 ppm acetone and low limit of 1 ppm at 190 ℃ is attributed to its uniform structure. Koo et al. (2018) also used ZIF-67 as a template to prepare NO_2 sensors out of WS_2 nanoplates coated with Co and an N-doped dodecahedral hollow carbon nanocage (HCNC), which has a polyhedron structure. Fig. 12a depicts the growth mechanism. The hollow polyhedron nanocage structure is shown in the TEM image of the WS_2_Co-N-HCNCs heat calcined at 700 ℃ (Fig. 12b). At room temperature, the sensor has the desired response (8.2% to 5 ppm) and NO_2 selectivity (Fig. 12c). The study demonstrated the potential for application of MOF templates in gas sensing.

ZIF-8 is also a suitable option for the fabrication of gas-sensitive materials. Li Z et al. (2020) designed NO_2 sensors based on In-doped ZnO porous hollow cages using ZIF-8 as a template. The sensor has a great response range (3.7 to 10 ppb) and a calculated detection limit of 0.2 ppb. Guo et al. (2021) used ZIF-8 as a template to create high-response TEA sensors based on PdO-ZnO-In_2O_3 nanofibers. Gas sensing performance was much improved due to the uniform structure of the ZIF-8 template and the catalytic capacity of PdO, which includes a fast response time (1 s) and a low detection limit (100 ppb).

Using $\{[Zn_5(L)_2(H_2O)_5]\cdot 7(DMA)\cdot 10(H_2O)_n\}$ (HPU-15) as a template, Li HJ et al. (2020) developed a diamond-shaped CuO/ZnO NP based methanol sensor. When exposed to methanol gas, the sensor performed admirably. The ZnO material based HPU-15 template, which is easily controlled, could be applied as a stable and selective sensing material.

4.5 Other templates

Other templates could be used to fabricate 3D nanomaterials with a complicated structure, resulting in a large specific surface area. Some common materials like plant templates (Zeng QR et al., 2020; Hong et al., 2022) and plant polyphenols (see supplementary materials, Sections 3), can be used as a template. Biomass with large holes and a stable internal structure, such as branches and straw, can also be applied, after treatment, as templates to generate 3D nanomaterials. For example, maize straw can be used as a template because it has a low cost, is readily available, and has a naturally porous structure. Zhang XM et al. (2017) used maize straw as a template to synthesize hierarchical structure ZnO:Ni NPs for an acetone sensor. The sensor demonstrated a high response

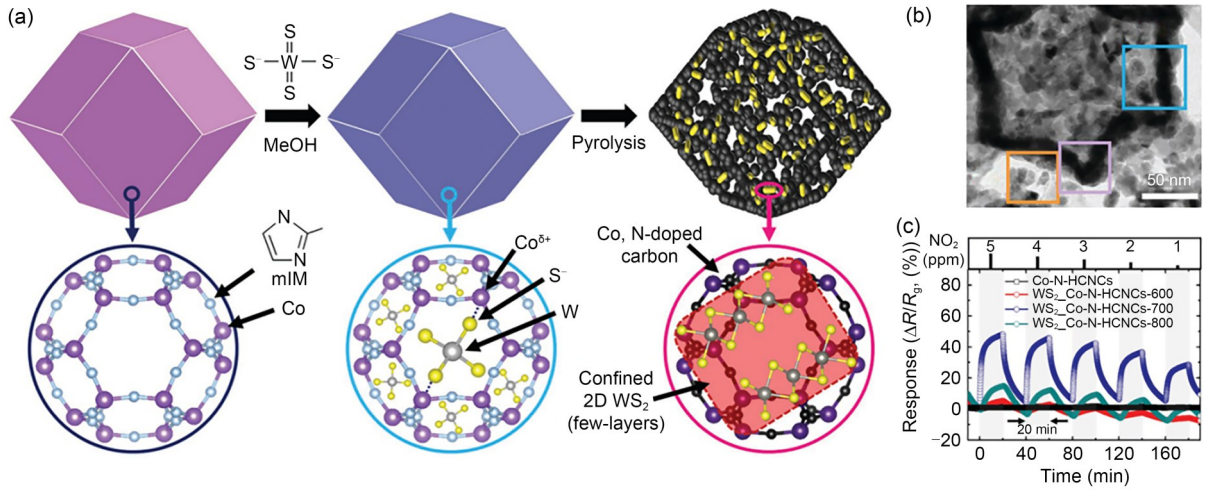

Fig. 12 Schematic of the process for synthesizing WS_2_Co-N-HCNCs (a), a transmission electron microscope (TEM) image of WS_2_Co-N-HCNCs-700 (b), and dynamic response curves of the sensors to 1–5 ppm NO_2 (c)

Reprinted from Koo et al. (2018), Copyright 2018, with permission from WILEY-VCH Verlag GmbH & Co. KGaA, Weinheim. 1 ppm=1×10^{-6}

and a fast response time/recovery time. Similarly, Teng et al. (2020) used low-cost poplar branches as a template to prepare a high-performance ppb-level H_2S sensor based on porous α-Fe_2O_3 tubules. The production process and the porous layered α-Fe_2O_3 tubule device are shown in Fig. 13a. As shown in Fig. 13b, the nanolamellar α-Fe_2O_3 supplants the porous hierarchically micro-tubular structure of the branch in the SEM image of samples calcined at 600 ℃ (Fe-600). The Fe-600 showed the greatest reaction to H_2S due to its unique hollow porous tubular structure inherited from the template (Fig. 13c). Fig. 13d shows that the nanolamellar α-Fe_2O_3 based sensor has the potential to determine decay of pork by detecting the concentration of H_2S.

The regular morphology and structure of 3D nanomaterials synthesized by templates are useful for improving the sensing performance of gas sensors. First, the hollow and porous 3D nanostructures promote gas molecule transfer and dramatically accelerate reaction rates. Second, the highly regular and homogeneous structure of NPs greatly increases the repeatability and long-term stability of gas sensors, extending their useful life. Finally, the large specific surface area provides more active sites, and the numerous gas diffusion channels aid gas diffusion, thereby improving detection accuracy. Based on these factors, 3D nanomaterials synthesized by templates have a lot of promise and might be widely used in gas sensing in the future.

5 Conclusions and outlook

In this review, the research progress of gas sensors based on template-assisted synthesis methods in recent years is summarized, including 1D, 2D, and 3D nanomaterials, as well as the morphology and properties of these materials synthesized by different templates, such as biomass, carbonaceous, and polymeric materials. For 1D nanomaterials, semiconductor nanomaterials prepared using the template-assisted method have a uniform morphology and complex surface structure, excellent gas diffusion, and a large number of active sites, efficiently accelerating the reaction rate, increasing the gas detection ability of the gas sensor, and ensuring long-term stability and repeatability. This

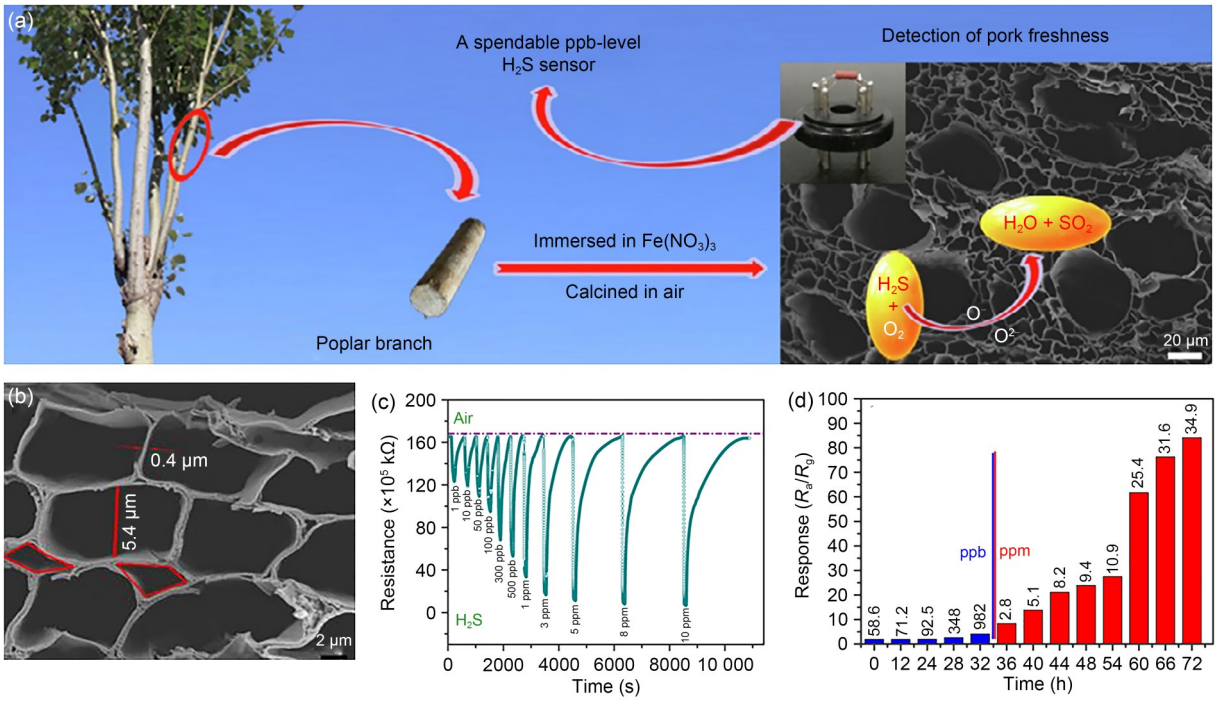

Fig. 13 Schematic of the synthesis process and sensing device of porous α-Fe_2O_3 tubules (a), a scanning electron microscope (SEM) image of Fe-600 (b), response/recovery curve to different concentrations of H_2S (c), and real-time detection of the H_2S concentration of pork at different time intervals (d)

Reprinted from Teng et al. (2020), Copyright 2019, with permission from Elsevier. 1 ppm=1×10^{-6}; 1 ppb=1×10^{-9}

shows that using the template-assisted synthesis method to increase the gas sensing capability of SMO NPs is a viable option. However, it is worthwhile to consider how the synthesis process and material selection could be improved to further enhance performance. For the future development of template-assisted synthesis methods, several important questions should be considered. First, many materials fabricated using a template can respond effectively, but the price of some template materials is high, which significantly increases the cost. Second, in many cases, the template treatment procedure is sophisticated and time-consuming. Furthermore, different surface treatments and reaction circumstances may change the template's fundamental capacity to guide material growth on the surface. Finally, the physicochemical features of the templates themselves can influence material production, leading to unexpected gas response test results. In terms of practical application, the template-assisted method will become more intuitive and convenient.

The field of gas sensors has made substantial use of the template-assisted synthesis technique. Looking ahead, the components of the template will develop toward high performance and low cost. For instance, the potential of biomass material, which is in line with the development path, cannot be overlooked as an inexpensive and environmentally beneficial resource. It could resolve many issues with the template-assisted method at this time due to its uniform structure and straightforward treatment process. However, compared to the usual template materials like MOFs and PS spheres, there has been little research on biomass material. Thus, there are still many important potential challenges in developing a strategy of combining template-assisted methods and recently discovered biomass materials suitable for creating gas sensors, and this strategy merits additional research. The development of template-assisted methods is likely to benefit from the discovery of new biomass materials in the future. Using template-assisted methods, particularly using biomass material as a template, will become an important strategy to create SMO-based gas sensors with low cost, low power consumption, and high performance in real time.

Contributors

Yuanyang XUN summarized the review. Feiyu ZHANG and Yan HONG drafted the paper. Ke XU and Ligang CHEN helped organize the paper. Siqi LI, Song LIU, and Bin LI revised and finalized the paper.

Compliance with ethics guidelines

Yuanyang XUN, Siqi LI, Feiyu ZHANG, Yan HONG, Ke XU, Ligang CHEN, Song LIU, and Bin LI declare that they have no conflict of interest.

References

Baek DH, Choi J, Kim J, 2019. Fabrication of suspended nanowires for highly sensitive gas sensing. *Sens Actuat B Chem*, 284:362-368. https://doi.org/10.1016/j.snb.2018.12.159

Bulemo PM, Cho HJ, Kim DH, et al., 2018. Facile synthesis of Pt-functionalized meso/macroporous SnO_2 hollow spheres through in situ templating with SiO_2 for H_2S sensors. *ACS Appl Mater Interfaces*, 10(21):18183-18191. https://doi.org/10.1021/acsami.8b00901

Chen J, Feng DL, Wang C, et al., 2020. Gas sensor detecting 3-hydroxy-2-butanone biomarkers: boosted response via decorating Pd nanoparticles onto the {010} facets of $BiVO_4$ decahedrons. *ACS Sens*, 5(8):2620-2627. https://doi.org/10.1021/acssensors.0c01149

Cheng PF, Lv L, Wang YL, et al., 2021. SnO_2/$ZnSnO_3$ double-shelled hollow microspheres based high-performance acetone gas sensor. *Sens Actuat B Chem*, 332:129212. https://doi.org/10.1016/j.snb.2020.129212

Escobedo P, Fernández-Ramos MD, López-Ruiz N, et al., 2022. Smart facemask for wireless CO_2 monitoring. *Nat Commun*, 13(1):72. https://doi.org/10.1038/s41467-021-27733-3

Fei HF, Long YD, Yu HJ, et al., 2020. Bimodal mesoporous carbon spheres with small and ultra-large pores fabricated using amphiphilic brush block copolymer micelle templates. *ACS Appl Mater Interfaces*, 12(51):57322-57329. https://doi.org/10.1021/acsami.0c16566

Gao ZM, Wang TQ, Li XF, et al., 2020. Pd-decorated PdO hollow shells: a H_2-sensing system in which catalyst nanoparticle and semiconductor support are interconvertible. *ACS Appl Mater Interfaces*, 12(38):42971-42981. https://doi.org/10.1021/acsami.0c13137

Giampiccolo A, Tobaldi DM, Leonardi SG, et al., 2019. Sol gel graphene/TiO_2 nanoparticles for the photocatalytic-assisted sensing and abatement of NO_2. *Appl Catal B Environ*, 243:183-194. https://doi.org/10.1016/j.apcatb.2018.10.032

Guo LL, Zhang B, Yang XL, et al., 2021. Sensing platform of PdO-ZnO-In_2O_3 nanofibers using MOF templated catalysts for triethylamine detection. *Sens Actuat B Chem*, 343:130126. https://doi.org/10.1016/j.snb.2021.130126

Hong SH, Song N, Jiang EH, et al., 2022. Nickel supported on nitrogen-doped biomass carbon fiber fabricated via in-situ template technology for pH-universal electrocatalytic hydrogen evolution. *J Colloid Interface Sci*, 608:1441-1448. https://doi.org/10.1016/j.jcis.2021.10.083

Hu CH, Yu LM, Li SL, et al., 2022. Sacrificial template triggered to synthesize hollow nanosheet-assembled Co_3O_4 microtubes for fast triethylamine detection. *Sens Actuat B Chem*, 355:131246. https://doi.org/10.1016/j.snb.2021.131246

Huang R, Zhu AM, Gong Y, et al., 2013. Facile method to prepare monodispersed hollow PtAu sphere with TiO_2 colloidal sphere as a template. *Ind Eng Chem Res*, 52(22):7432-7438. https://doi.org/10.1021/ie400573c

Hung PS, Chou YS, Huang BH, et al., 2020. A vertically integrated ZnO-based hydrogen sensor with hierarchical bilayered inverse opals. *Sens Actuat B Chem*, 325:128779. https://doi.org/10.1016/j.snb.2020.128779

Ivanova A, Frka-Petesic B, Paul A, et al., 2020. Cellulose nanocrystal-templated tin dioxide thin films for gas sensing. *ACS Appl Mater Interfaces*, 12(11):12639-12647. https://doi.org/10.1021/acsami.9b11891

Jang JS, Koo WT, Choi SJ, et al., 2017. Metal organic framework-templated chemiresistor: sensing type transition from P-to-N using hollow metal oxide polyhedron via galvanic replacement. *J Am Chem Soc*, 139(34):11868-11876. https://doi.org/10.1021/jacs.7b05246

Jo YK, Jeong SY, Moon YK, et al., 2021. Exclusive and ultrasensitive detection of formaldehyde at room temperature using a flexible and monolithic chemiresistive sensor. *Nat Commun*, 12(1):4955. https://doi.org/10.1038/s41467-021-25290-3

Kim DH, Kim SJ, Shin H, et al., 2019. High-resolution, fast, and shape-conformable hydrogen sensor platform: polymer nanofiber yarn coupled with nanograined Pd@Pt. *ACS Nano*, 13(5):6071-6082. https://doi.org/10.1021/acsnano.9b02481

Kim DH, Cha JH, Lim JY, et al., 2020. Colorimetric dye-loaded nanofiber yarn: eye-readable and weavable gas sensing platform. *ACS Nano*, 14(12):16907-16918. https://doi.org/10.1021/acsnano.0c05916

Kim S, Singh G, Oh M, et al., 2021. An analysis of a highly sensitive and selective hydrogen gas sensor based on a 3D Cu-doped SnO_2 sensing material by efficient electronic sensor interface. *ACS Sens*, 6(11):4145-4155. https://doi.org/10.1021/acssensors.1c01696

Koo WT, Cha JH, Jung JW, et al., 2018. Few-layered WS_2 nanoplates confined in Co, N-doped hollow carbon nanocages: abundant WS_2 edges for highly sensitive gas sensors. *Adv Funct Mater*, 28(36):1802575. https://doi.org/10.1002/adfm.201802575

Li C, Qiao XK, Jian J, et al., 2019. Ordered porous $BiVO_4$ based gas sensors with high selectivity and fast-response towards H_2S. *Chem Eng J*, 375:121924. https://doi.org/10.1016/j.cej.2019.121924

Li HJ, Zhang N, Zhao XL, et al., 2020. Modulation of TEA and methanol gas sensing by ion-exchange based on a sacrificial template 3D diamond-shaped MOF. *Sens Actuat B Chem*, 315:128136. https://doi.org/10.1016/j.snb.2020.128136

Li L, Tan JF, Dun MH, et al., 2017. Porous $ZnFe_2O_4$ nanorods with net-worked nanostructure for highly sensor response and fast response acetone gas sensor. *Sens Actuat B Chem*, 248:85-91. https://doi.org/10.1016/j.snb.2017.03.119

Li Q, Wu JB, Huang L, et al., 2018. Sulfur dioxide gas-sensitive materials based on zeolitic imidazolate framework-derived carbon nanotubes. *J Mater Chem A*, 6(25):12115-12124. https://doi.org/10.1039/c8ta02036a

Li RF, Qi H, Ma Y, et al., 2020. A flexible and physically transient electrochemical sensor for real-time wireless nitric oxide monitoring. *Nat Commun*, 11(1):3207. https://doi.org/10.1038/s41467-020-17008-8

Li Z, Zhang Y, Zhang H, et al., 2020. Superior NO_2 sensing of MOF-derived indium-doped ZnO porous hollow cages. *ACS Appl Mater Interfaces*, 12(33):37489-37498. https://doi.org/10.1021/acsami.0c10420

Li Z, Zhang Y, Zhang H, et al., 2021. MOF-derived Au-loaded Co_3O_4 porous hollow nanocages for acetone detection. *Sens Actuat B Chem*, 344:130182. https://doi.org/10.1016/j.snb.2021.130182

Liang ZB, Qu C, Zhou WY, et al., 2019. Synergistic effect of Co-Ni hybrid phosphide nanocages for ultrahigh capacity fast energy storage. *Adv Sci*, 6(8):1802005. https://doi.org/10.1002/advs.201802005

Lin LS, Yang XY, Zhou ZJ, et al., 2017. Yolk-shell nanostructure: an ideal architecture to achieve harmonious integration of magnetic-plasmonic hybrid theranostic platform. *Adv Mater*, 29(21):1606681. https://doi.org/10.1002/adma.201606681

Liu W, Xu L, Sheng K, et al., 2018. A highly sensitive and moisture-resistant gas sensor for diabetes diagnosis with Pt@In_2O_3 nanowires and a molecular sieve for protection. *NPG Asia Mater*, 10(4):293-308. https://doi.org/10.1038/s41427-018-0029-2

Liu WX, Sun JB, Li YN, et al., 2023. Low-temperature and high-selectivity butanone sensor based on porous Fe_2O_3 nanosheets synthesized by phoenix tree leaf template. *Sens Actuat B Chem*, 377:133054. https://doi.org/10.1016/j.snb.2022.133054

Liu XJ, Duan XP, Zhang C, et al., 2022. Improvement toluene detection of gas sensors based on flower-like porous indium oxide nanosheets. *J Alloys Compd*, 897:163222. https://doi.org/10.1016/j.jallcom.2021.163222

Lu JJ, Liu DP, Zhou JC, et al., 2017. Porous organic field-effect transistors for enhanced chemical sensing performances. *Adv Funct Mater*, 27(20):1700018. https://doi.org/10.1002/adfm.201700018

Luong HM, Pham MT, Guin T, et al., 2021. Sub-second and ppm-level optical sensing of hydrogen using templated control of nano-hydride geometry and composition. *Nat Commun*, 12(1):2414. https://doi.org/10.1038/s41467-021-22697-w

Lv L, Cheng PF, Wang YL, et al., 2020. Sb-doped three-dimensional $ZnFe_2O_4$ macroporous spheres for N-butanol chemiresistive gas sensors. *Sens Actuat B Chem*, 320:128384. https://doi.org/10.1016/j.snb.2020.128384

Ma JW, Fan HQ, Zhang WM, et al., 2020. High sensitivity and ultra-low detection limit of chlorine gas sensor based on In_2O_3 nanosheets by a simple template method. *Sens Actuat B Chem*, 305:127456. https://doi.org/10.1016/j.snb.2019.127456

Masoumi S, Shokrani M, Aghili S, et al., 2019. Zinc oxide-based direct thermoelectric gas sensor for the detection of volatile organic compounds in air. *Sens Actuat B Chem*, 294:245-252. https://doi.org/10.1016/j.snb.2019.05.063

Na HB, Zhang XF, Zhang M, et al., 2019a. A fast response/recovery ppb-level H_2S gas sensor based on porous CuO/ZnO

heterostructural tubule via confined effect of absorbent cotton. *Sens Actuat B Chem*, 297:126816. https://doi.org/10.1016/j.snb.2019.126816

Na HB, Zhang XF, Deng ZP, et al., 2019b. Large-scale synthesis of hierarchically porous ZnO hollow tubule for fast response to ppb-level H_2S gas. *ACS Appl Mater Interfaces*, 11(12):11627-11635. https://doi.org/10.1021/acsami.9b00173

Nasir ME, Dickson W, Wurtz GA, et al., 2014. Hydrogen detected by the naked eye: optical hydrogen gas sensors based on core/shell plasmonic nanorod metamaterials. *Adv Mater*, 26(21):3532-3537. https://doi.org/10.1002/adma.201305958

Ogbeide O, Bae G, Yu WB, et al., 2022. Inkjet-printed rGO/binary metal oxide sensor for predictive gas sensing in a mixed environment. *Adv Funct Mater*, 32(25):2113348. https://doi.org/10.1002/adfm.202113348

Park SW, Jeong SY, Yoon JW, et al., 2020. General strategy for designing highly selective gas-sensing nanoreactors: morphological control of SnO_2 hollow spheres and configurational tuning of Au catalysts. *ACS Appl Mater Interfaces*, 12(46):51607-51615. https://doi.org/10.1021/acsami.0c13760

Sabri YM, Kandjani AE, Rashid SSAAH, et al., 2018. Soot template TiO_2 fractals as a photoactive gas sensor for acetone detection. *Sens Actuat B Chem*, 275:215-222. https://doi.org/10.1016/j.snb.2018.08.059

Sanger A, Kang SB, Jeong MH, et al., 2018. Morphology-controlled aluminum-doped zinc oxide nanofibers for highly sensitive NO_2 sensors with full recovery at room temperature. *Adv Sci*, 5(9):1800816. https://doi.org/10.1002/advs.201800816

Seo MH, Kang K, Yoo JY, et al., 2020. Chemo-mechanically operating palladium-polymer nanograting film for a self-powered H_2 gas sensor. *ACS Nano*, 14(12):16813-16822. https://doi.org/10.1021/acsnano.0c05476

Sharma B, Sharma A, Myung JH, 2021. Selective ppb-level NO_2 gas sensor based on SnO_2-boron nitride nanotubes. *Sens Actuat B Chem*, 331:129464 https://doi.org/10.1016/j.snb.2021.129464

Shin H, Lee WJ, 2016. Multi-shelled $MgCo_2O_4$ hollow microspheres as anodes for lithium ion batteries. *J Mater Chem A*, 4(31):12263-12272. https://doi.org/10.1039/c6ta03959f

Shin H, Kim DH, Jung W, et al., 2021. Surface activity-tuned metal oxide chemiresistor: toward direct and quantitative halitosis diagnosis. *ACS Nano*, 15(9):14207-14217. https://doi.org/10.1021/acsnano.1c01350

Sun ZQ, Liao T, Dou YH, et al., 2014. Generalized self-assembly of scalable two-dimensional transition metal oxide nanosheets. *Nat Commun*, 5:3813. https://doi.org/10.1038/ncomms4813

Tammanoon N, Iwamoto T, Ueda T, et al., 2020. Synergistic effects of PdO_x-CuO_x loadings on methyl mercaptan sensing of porous WO_3 microspheres prepared by ultrasonic spray pyrolysis. *ACS Appl Mater Interfaces*, 12(37):41728-41739. https://doi.org/10.1021/acsami.0c10462

Tan CL, Zhang H, 2015. Wet-chemical synthesis and applications of non-layer structured two-dimensional nanomaterials. *Nat Commun*, 6:7873. https://doi.org/10.1038/ncomms8873

Teng Y, Zhang XF, Xu TT, et al., 2020. A spendable gas sensor with higher sensitivity and lowest detection limit towards H_2S: porous α-Fe_2O_3 hierarchical tubule derived from poplar branch. *Chem Eng J*, 392:123679. https://doi.org/10.1016/j.cej.2019.123679

Tie Y, Ma SY, Pei ST, et al., 2020. Pr doped $BiFeO_3$ hollow nanofibers via electrospinning method as a formaldehyde sensor. *Sens Actuat B Chem*, 308:127689. https://doi.org/10.1016/j.snb.2020.127689

Wang H, Luo YY, Li K, et al., 2022. Porous α-Fe_2O_3 gas sensor with instantaneous attenuated response toward triethylamine and its reaction kinetics. *Chem Eng J*, 427:131631. https://doi.org/10.1016/j.cej.2021.131631

Wang L, Sun LY, Bian FK, et al., 2022. Self-bonded hydrogel inverse opal particles as sprayed flexible patch for wound healing. *ACS Nano*, 16(2):2640-2650. https://doi.org/10.1021/acsnano.1c09388

Wang Q, Wu HC, Wang YR, et al., 2021. Ex-situ XPS analysis of yolk-shell Sb_2O_3/WO_3 for ultra-fast acetone resistive sensor. *J Hazard Mater*, 412:125175. https://doi.org/10.1016/j.jhazmat.2021.125175

Wang TS, Jiang B, Yu Q, et al., 2019. Realizing the control of electronic energy level structure and gas-sensing selectivity over heteroatom-doped In_2O_3 spheres with an inverse opal microstructure. *ACS Appl Mater Interfaces*, 11(9):9600-9611. https://doi.org/10.1021/acsami.8b21543

Wen ZY, Ren HB, Li DX, et al., 2023. A highly efficient acetone gas sensor based on 2D porous $ZnFe_2O_4$ nanosheets. *Sens Actuat B Chem*, 379:133287. https://doi.org/10.1016/j.snb.2023.133287

Wu YY, Song BY, Zhang XF, et al., 2021. Microtubular α-Fe_2O_3/$Fe_2(MoO_4)_3$ heterostructure derived from absorbent cotton for enhanced ppb-level H_2S gas-sensing performance. *J Alloys Compd*, 867:158994. https://doi.org/10.1016/j.jallcom.2021.158994

Xia Y, Zhou LX, Yang J, et al., 2020. Highly sensitive and fast optoelectronic room-temperature NO_2 gas sensor based on ZnO nanorod-assembled macro-/mesoporous film. *ACS Appl Electron Mater*, 2(2):580-589. https://doi.org/10.1021/acsaelm.9b00810

Xie WH, Ren Y, Yu BJ, et al., 2021. Self-hybrid transition metal oxide nanosheets synthesized by a facile programmable and scalable carbonate-template method. *Small*, 17(39):2103176. https://doi.org/10.1002/smll.202103176

Xiong Y, Zhu ZY, Ding DG, et al., 2018. Multi-shelled $ZnCo_2O_4$ yolk-shell spheres for high-performance acetone gas sensor. *Appl Surf Sci*, 443:114-121. https://doi.org/10.1016/j.apsusc.2018.02.189

Xu SP, Sun FQ, Gu FL, et al., 2014. Photochemistry-based method for the fabrication of SnO_2 monolayer ordered porous films with size-tunable surface pores for direct application in resistive-type gas sensor. *ACS Appl Mater Interfaces*, 6(2):1251-1257. https://doi.org/10.1021/am4050844

Xue MQ, Li FW, Chen D, et al., 2016. High-oriented polypyrrole nanotubes for next-generation gas sensor. *Adv Mater*, 28(37):8265-8270. https://doi.org/10.1002/adma.201602302

Yang JQ, Han WJ, Ma J, et al., 2021. Sn doping effect on NiO hollow nanofibers based gas sensors about the humidity dependence for triethylamine detection. *Sens Actuat B Chem*, 340:129971. https://doi.org/10.1016/j.snb.2021.129971

Yang S, Sun J, Xu L, et al., 2020. Au@ZnO functionalized three-dimensional macroporous WO_3: a application of selective H_2S gas sensor for exhaled breath biomarker detection. *Sens Actuat B Chem*, 324:128725. https://doi.org/10.1016/j.snb.2020.128725

Yang XY, Shi YT, Xie KF, et al., 2022. Cocrystallization enabled spatial self-confinement approach to synthesize crystalline porous metal oxide nanosheets for gas sensing. *Angew Chem Int Ed*, 61(37):e202207816. https://doi.org/10.1002/anie.202207816

Yao Y, Yin ML, Yan JQ, et al., 2017. Controllable synthesis of Ag-WO_3 core-shell nanospheres for light-enhanced gas sensors. *Sens Actuat B Chem*, 251:583-589. https://doi.org/10.1016/j.snb.2017.05.007

Yi SY, Song YG, Park JY, et al., 2019. Morphological evolution induced through a heterojunction of W-decorated NiO nanoigloos: synergistic effect on high-performance gas sensors. *ACS Appl Mater Interfaces*, 11(7):7529-7538. https://doi.org/10.1021/acsami.8b18678

Yuan HY, Aljneibi SAAA, Yuan JR, et al., 2019. ZnO nanosheets abundant in oxygen vacancies derived from metal-organic frameworks for ppb-level gas sensing. *Adv Mater*, 31(11): 1807161. https://doi.org/10.1002/adma.201807161

Yuan KP, Wang CY, Zhu LY, et al., 2020. Fabrication of a microelectromechanical system-based acetone gas sensor using CeO_2 nanodot-decorated WO_3 nanowires. *ACS Appl Mater Interfaces*, 12(12):14095-14104. https://doi.org/10.1021/acsami.9b18863

Zeng G, Wu C, Chang Y, et al., 2019. Detection and discrimination of volatile organic compounds using a single film bulk acoustic wave resonator with temperature modulation as a multiparameter virtual sensor array. *ACS Sens*, 4(6): 1524-1533. https://doi.org/10.1021/acssensors.8b01678

Zeng QR, Feng JT, Lin XC, et al., 2020. One-step facile synthesis of a NiO/ZnO biomorphic nanocomposite using a poplar tree leaf template to generate an enhanced gas sensing platform to detect n-butanol. *J Alloys Compd*, 815:150550. https://doi.org/10.1016/j.jallcom.2019.05.018

Zhang B, Sun JY, Gao PX, 2021. Low-concentration NO_x gas analysis using single bimodular ZnO nanorod sensor. *ACS Sens*, 6(8):2979-2987. https://doi.org/10.1021/acssensors.1c00834

Zhang LH, Dong B, Xu L, et al., 2017. Three-dimensional ordered ZnO-Fe_3O_4 inverse opal gas sensor toward trace concentration acetone detection. *Sens Actuat B Chem*, 252:367-374. https://doi.org/10.1016/j.snb.2017.05.167

Zhang XM, Dong ZJ, Liu SR, et al., 2017. Maize straw-templated hierarchical porous ZnO: Ni with enhanced acetone gas sensing properties. *Sens Actuat B Chem*, 243: 1224-1230. https://doi.org/10.1016/j.snb.2016.12.076

Zhao C, Zhou AW, Dou YB, et al., 2021. Dual MOFs template-directed fabrication of hollow-structured heterojunction photocatalysts for efficient CO_2 reduction. *Chem Eng J*, 416:129155. https://doi.org/10.1016/j.cej.2021.129155

Zhao RJ, Zhang X, Peng SJ, et al., 2020. Shaddock peels as bio-templates synthesis of Cd-doped SnO_2 nanofibers: a high performance formaldehyde sensing material. *J Alloys Compd*, 813:152170. https://doi.org/10.1016/j.jallcom.2019.152170

Zheng XZ, Zhang Z, Meng SG, et al., 2020. Regulating charge transfer over 3D Au/ZnO hybrid inverse opal toward efficiently photocatalytic degradation of bisphenol A and photoelectrochemical water splitting. *Chem Eng J*, 393:124676. https://doi.org/10.1016/j.cej.2020.124676

Zheng YY, Wang LQ, Tian HW, et al., 2021. Bimetal carbonaceous templates for multi-shelled $NiCo_2O_4$ hollow sphere with enhanced xylene detection. *Sens Actuat B Chem*, 339: 129862. https://doi.org/10.1016/j.snb.2021.129862

Zhu XQ, Li J, Ali RN, et al., 2018. Toward a high-performance Li-ion battery: constructing a $Co_{1-x}S$/ZnS@C composite derived from metal-organic framework @3D disordered polystyrene sphere template. *Mater Des*, 160:636-641. https://doi.org/10.1016/j.matdes.2018.10.011

List of supplementary materials